Haigh, I. D., M. Eliot, and C. Pattiaratchi (2011), Global influences of the 18.61 year nodal cycle and 8.85 year cycle of lunar perigee on high tidal levels, J. Geophys. Res., 116, C06025, doi: 10.1029/2010JC006645.

Global influences of the 18.61 year nodal cycle and 8.85 year cycle of lunar perigee on high tidal levels

Ivan D. Haigh,[1] Matt Eliot,[1] and Charitha Pattiaratchi[1]

Received 8 September 2010; revised 3 March 2011; accepted 16 March 2011; published 29 June 2011.

[1] Periods of high astronomically generated tides contribute to the occurrence of extreme sea levels. Over interannual time scales, two precessions associated with the orbit of the Moon cause systematic variation of high tides. A global assessment of when these tidal modulations occur allows for the prediction of periods when the enhanced risk of coastal flooding is likely in different parts of the world. This paper uses modeled tides to assess the influence of the 18.61 year lunar nodal cycle and the 8.85 year cycle of lunar perigee (which affects high tidal levels as a quasi 4.4 year cycle) on high tidal levels on a global scale. Tidal constituents from the TPXO7.2 global tidal model are used, with satellite modulation corrections based on equilibrium tide expectations, to predict multidecadal hourly time series of tides on a one-quarter degree global grid. These time series are used to determine the amplitude and phase of tidal modulations using harmonic analysis fitted to 18.61, 9.305, 8.85, and 4.425 year sinusoidal signals. The spatial variations in the range and phase of the tidal modulations are related to the global distribution of the main tidal constituents and tidal characteristics (diurnal or semidiurnal and tidal range). Results indicate that the 18.61 year nodal cycle has the greatest influence in diurnal regions with tidal ranges of >4 m and that the 4.4 year cycle is largest in semidiurnal regions where the tidal range is >6 m. The phase of the interannual tidal modulations is shown to relate to the form of the tide.

Citation: Haigh, I. D., M. Eliot, and C. Pattiaratchi (2011), Global influences of the 18.61 year nodal cycle and 8.85 year cycle of lunar perigee on high tidal levels, *J. Geophys. Res.*, *116*, C06025, doi:10.1029/2010JC006645.

1. Introduction

[2] When extreme sea level events occur along low-lying, highly populated, and/or developed coastlines, the impacts can be devastating, including considerable loss of life, billions of dollars worth of damage, and drastic changes to coastal landforms [*Lowe et al.*, 2010]. As a society, we have become increasingly vulnerable to extreme high sea levels because of the rapid growth in coastal populations and the accompanying increased investment in infrastructure at the coastal zone [*Nicholls et al.*, 2007]. The occurrences of major coastal floods in the last decade (i.e., those arising from hurricanes Katrina, Sidr, and Nargis) have dramatically emphasized the damage that extreme sea level events are capable of, particularly when combined with the rise in coastal populations [*Menéndez and Woodworth*, 2010].

[3] Extreme sea levels (exclusive of surface gravity waves) arise as a combination of three factors: mean sea level, tide, and surge [*Pugh*, 2004]. Extreme sea levels are most often viewed in the context of storm surges, but the impacts of storm events in many coastal areas are strongly modulated by the tide [*Wood*, 2001a]. Over interannual time scales, variations in high tides arise as a result of the 18.61 year lunar nodal cycle and the 8.85 year cycle of lunar perigee, the latter of which influences sea level as a quasi 4.4 year cycle [*Wood*, 2001b; *Woodworth and Blackman*, 2004; *Menéndez and Woodworth*, 2010]. Assessment of these systematic tidal modulations allows the prediction of periods when enhanced risk of coastal flooding is likely.

[4] Recently, *Eliot* [2010] examined the influence of interannual tidal modulations on coastal flooding along the Western Australian coastline using tide gauge observations. Interestingly, his results indicated that the contribution of tidal modulations to the likelihood with which high water levels would be exceeded varied significantly around the coastline in terms of both amplitude and phase. High water levels along the southern part of the coastline were dominated by the nodal cycle, while the northwest region was affected mainly by the quasi 4.4 year cycle of perigean influence. In the microtidal southwest region of Western Australia, the lunar nodal cycle had a range (i.e., twice the amplitude) of about 10 cm in high tidal levels, which is small compared to the surge and mean sea level fluctuations. However, on the basis of the return period curves calculated from tide gauge records in this region, *Eliot* [2010] showed that a 10 cm rise in water level represents a threefold variation in the relative likelihood of extreme flood events. *Eliot* [2010] also emphasized that the phases of the interannual tidal modulations are significant. The nodal modulation was detected in the records for the northern part of the coastline,

[1]School of Environmental Systems Engineering and UWA Oceans Institute, University of Western Australia, Crawley, Western Australia, Australia.

0148-0227/11/2010JC006645

but this was 180° out of phase with the nodal modulations detected in tide gauge records in the southern region. The most recent peaks of the nodal modulations occurred in 1997 for northern sites and in 2006 for southern sites. These different features of high tidal levels around Western Australia are important from a flood management point of view, and their effects contribute to the year-to-year variation of coastal management requirements.

[5] The aim of this paper is to examine the contribution of the 18.61 year lunar nodal cycle and the 8.85 year cycle of lunar perigee to high tidal levels on a global scale. Tidal constituents from a global tidal model are used, in conjunction with satellite modulation corrections based on equilibrium expectations, to predict multidecadal hourly tidal time series. From these long time series, the amplitude and phase of the two interannual tidal cycles and their subharmonics are calculated for different high tidal levels. The locations where they most influence high tidal levels are identified. The spatial variations in the range and phase of the modulations in high tidal levels are related to the global distribution of the main tidal constituents and tidal characteristics (diurnal/semidiurnal and tidal range).

2. Background

[6] Tidal modulations are systematic variations of tidal forcing mainly caused by the relative movements of the Earth, Moon, and Sun, with the spring-neap cycle being the most commonly recognized. Two important precessions (a precession is defined as the rotation of a plane with respect to a reference plane) of the Moon, namely, the 18.61 year lunar nodal cycle and the 8.85 year cycle of lunar perigee, cause tidal modulations on interannual time scales. These modulations affect the interpretation of tide gauge records that extend over several years, particularly when dealing with water level extremes [e.g., *Kaye and Stuckey*, 1973; *Wood*, 2001b; *Woodworth and Blackman*, 2004; *Araújo and Pugh*, 2008; *Haigh et al.*, 2010; *Menéndez and Woodworth*, 2010]. A brief description of the two cycles, their influence on tidal forcing, and the methods for inclusion in tidal analyses are given here. None of this material is new.

[7] The lunar nodal cycle was defined by *Bradley* [1728]; it is determined by the relative movement of the plane in which the Moon orbits the Earth [*Pugh*, 1987]. This orbital plane is inclined at 5°9′ to the plane in which the Earth orbits the Sun (this plane is called the ecliptic), which is inclined at 23°27′ to the Earth's equatorial plane. The point where the Moon crosses from the south to the north of the ecliptic is called the Moon's ascending node [*Ray*, 2007]. The mean longitude of the ascending node (denoted N) is calculated relative to the vernal equinox, one of two points where the Earth's equator intersects the ecliptic. Primarily because of the gravitational attraction by the Sun, the Moon's orbital plane precesses in a retrograde sense so that, with time, the rate of change of N is negative (i.e., westward) [see *Ray*, 2007, Figure B1]. The period of precessions is 18.61 years. It is for this reason that a draconic month (the time it takes for the Moon to return to the same node) is shorter than the sidereal month (the time it takes for the Moon to complete one revolution with respect to the fixed stars). This motion is often referred to as the "regression of the Moon's nodes." The longitude N can be evaluated by the formula [*Pugh*, 1987]

$$N(T) = 259.16^\circ - 1934.14^\circ T + 0.0021^\circ T^2,$$

where T is the number of Julian centuries that have passed since midnight on 1 January 1900 at the Greenwich meridian.

[8] The 18.61 year lunar nodal precession has a large effect on the Moon's declination (its angle below or above the equator), maximizing the declination when $N = 0°$ ($23° 27′ + 5°9′ = 28°36′$) and minimizing it when $N = 180°$ ($23° 27′ - 5°9′ = 18°18′$) [see *Ray*, 2007, Figure B1]. In the latter part of the 20th century and early part of the 21st century, N crossed 0° (i.e., lunar declination reached maxima) in March 1969, November 1987, and June 2006. N crossed 180° (i.e., lunar declination reached minima) in July 1978 and March 1997 and will cross 180° again in October 2015. Changes in the Moon's declination, in turn, have a large effect on the character of lunar tidal forcing. A large declination tends to maximize diurnal forces at the expense of semidiurnal and vice versa [*Ray*, 2007].

[9] The cycle of lunar perigee is determined by the Moon's elliptical orbit around the Earth, with its phase described by the positions of least and greatest distance known as perigee and apogee, respectively [*Pugh*, 1987]. The line joining perigee and apogee (the line of apsides) advances in the opposite direction of the lunar regression (i.e., eastward) and completes a full revolution in 8.85 years. It is for this reason that the anomalistic month (the period of time that the Moon moves from the perigee to the apogee and to the perigee again) is longer than the sidereal month. The longitude of lunar perigee (p) can be evaluated by the formula [*Pugh*, 1987]

$$p(T) = 334.39^\circ - 4069.04^\circ T + 0.0103^\circ T^2,$$

where T is the number of Julian centuries that have passed since midnight on 1 January 1900 at the Greenwich meridian.

[10] The main influence of the 8.85 year cycle of lunar perigee on high tides occurs as a quasi 4.4 year cycle. About every 4.4 years, the Sun is coincident with the line of apsides. Larger tidal ranges are experienced during these years, particularly around the time of the equinox when the Sun's declination is zero (which maximizes semidiurnal forces) [*Cartwright*, 1974; *Wood*, 2001a].

[11] Tidal modulations are developed through variations in the gravitational tidal potential in response to the relative positions of the Moon, Earth, and Sun [*Pugh*, 1987]. The influence of these modulations upon the frequency and range of high water levels is determined by their relative direction of variation and the source of the high water levels. In general, the high water levels may be classed according to the dominant semidiurnal or diurnal tidal form. Both nodal and perigean influences may be present for either tidal form; however, there is a general association of perigean influence on high water levels for areas with mainly semidiurnal tides and a general association of nodal influence on high water levels for areas with mainly diurnal tides.

[12] The 18.61 year lunar nodal cycle represents variation of lunar declination, which therefore enhances the latitudinal

Table 1. Satellite Modulation Correction Terms for the Lunar Constituents[a]

	f (Factor)	u (Angle) (deg)
M_m	$1.000 - 0.130\cos(N)$	0.0°
M_f	$1.043 + 0.414\cos(N)$	$-23.7°\sin(N)$
Q_1, O_1	$1.009 + 0.187\cos(N)$	$10.8°\sin(N)$
K_1	$1.006 + 0.115\cos(N)$	$-8.9°\sin(N)$
M_2, N_2	$1.000 - 0.037\cos(N)$	$-2.1°\sin(N)$
K_2	$1.024 + 0.286\cos(N)$	$-17.7°\sin(N)$

[a][After *Pugh* [1987, Table 4:3]. N is the longitude of the Moon's ascending node. The diurnal terms, M_f and K_2, have maximum amplitudes when $N = 0°$ in March 1969, November 1987, June 2006, etc., when M_2 is at a minimum. M_2, N_2, and M_m have maximum equilibrium amplitudes when $N = 180°$ in July 1978, March 1997, October 2015, etc.

influence of diurnal inequality and solstitial tides. Hence, the nodal cycle more strongly influences high water level variation in regions principally experiencing diurnal tides, with peaks at the solstices. The 8.85 year perigean cycle represents variation of lunar orientation relative to the Earth-Sun axis, and therefore, it is mainly a "longitudinal" motion. Enhanced tidal forcing occurs when there is Earth-Sun-Moon alignment in both longitude and declination, with the latter mechanism producing equinoctial peak tides for regions experiencing mainly semidiurnal tides. As the solar declination is away from the equator during the solstices, the perigean cycle does not produce a regular harmonic influence on high water levels in regions experiencing mainly diurnal tides.

[13] The effects of the lunar nodal and perigean modulations on individual tidal constituents are well understood and routinely allowed for in tidal analyses of sea level data.

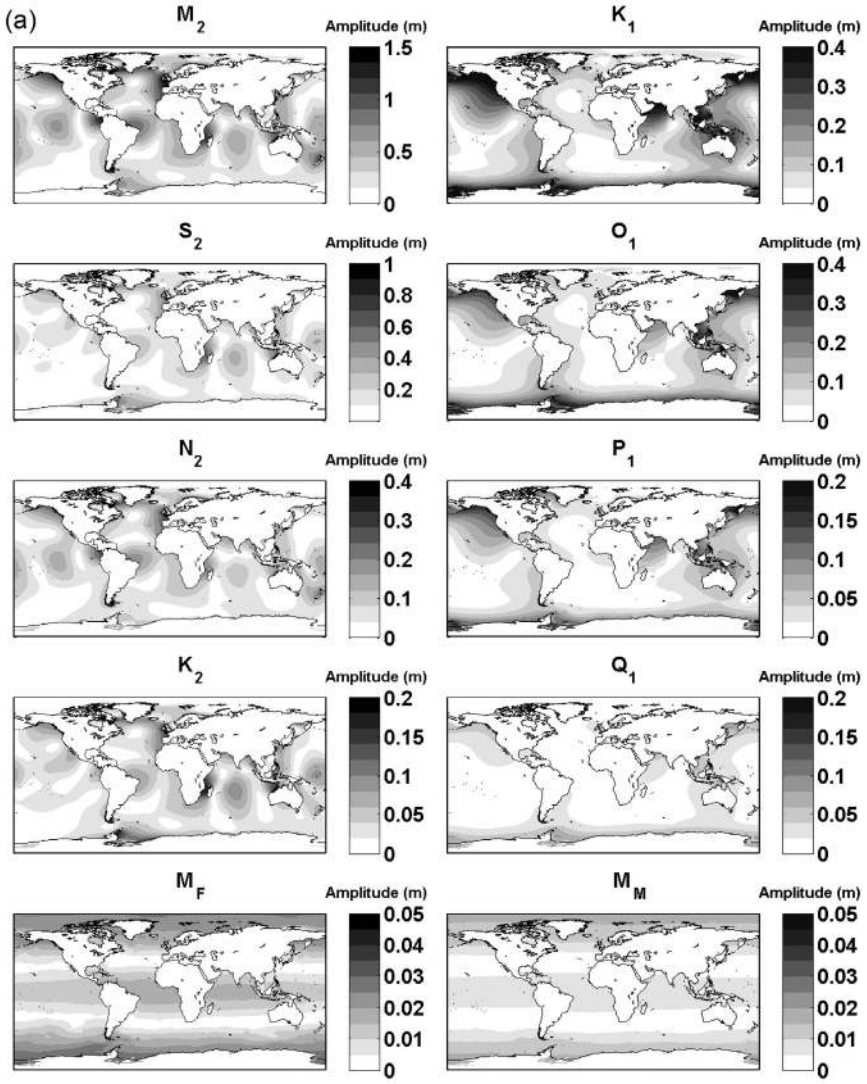

Figure 1. (a) Amplitude of the eight primary and two long-period tidal constituents from the TPXO7.2 global tidal model. (b) Amplitude of these constituents multiplied by the satellite modulation corrections listed in Table 1. Note that the shading scales are different in Figure 1a but are the same in Figure 1b.

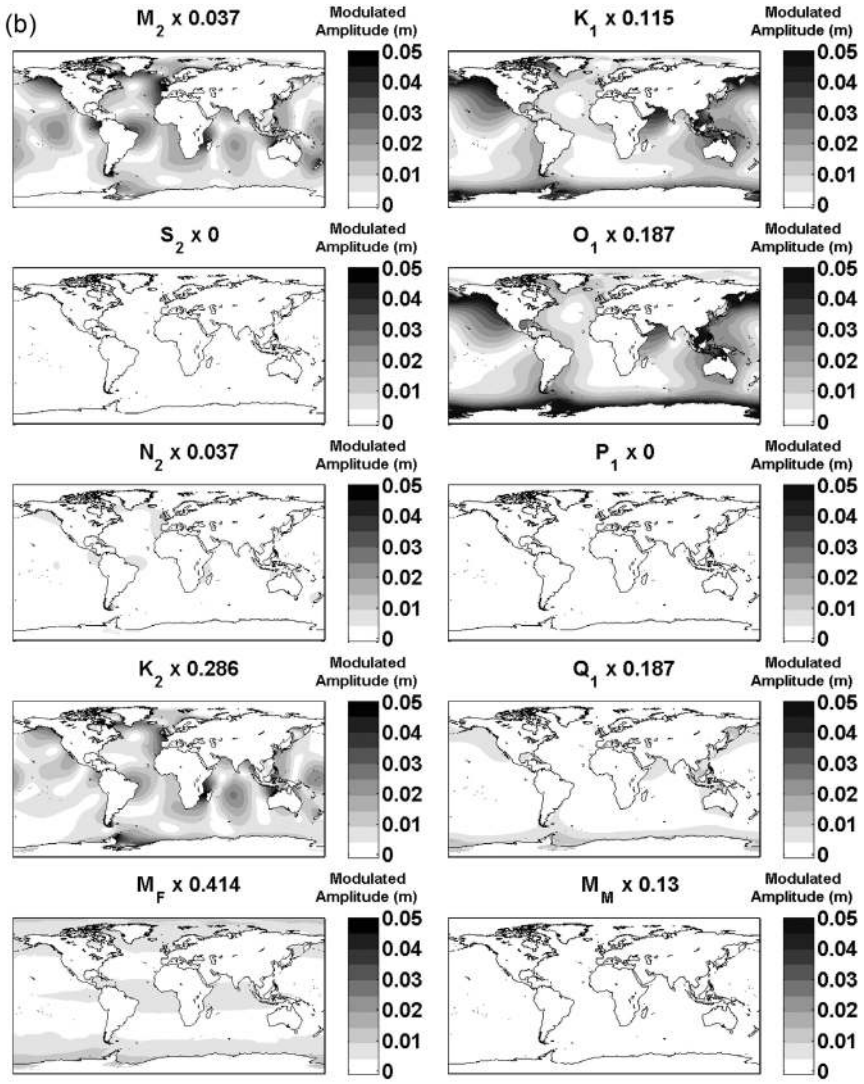

Figure 1. (continued)

In modern harmonic analyses of tidal heights [*Godwin*, 1972; *Foreman*, 1977; *Pugh*, 1987], which follow the development of tidal potential theory by *Doodson* [1921], the frequency of each tidal constituent is expressed as a linear superposition of six astronomical forcing harmonics of the form [*Cherniawsky et al.*, 2010]

$$\omega_k = l_1\tau + l_2 s + l_3 h + l_4 p + l_5 N + l_6 p',$$

where l_i are small integers known as Doodson numbers; τ, s, and h are the mean rates of change of lunar time (with a mean period of 24.84 h) and of the longitudes of the Moon (27.3 days) and the Sun (365.24 days), respectively; p and $-N$, as outlined above, are the mean longitude of the lunar perigee (8.85 years) and of the Moon's ascending node (18.61 years), respectively; and p' is the solar perigee (20,392 years), which is similar in nature to the lunar perigee motion but is determined by the Earth's elliptic orbit around the Sun. (The influence of the solar perigee cycle on high tidal levels is negligible over the time scales considered in this paper.) From the six variables τ, s, h, p, N, and p', one can calculate the positions of the Sun or Moon, and hence the tidal generating forces, at any time [*Foreman*, 1977].

[14] *Cartwright and Edden* [1973] showed in detail how the major tidal constituents (the technical definition of a tidal constituent is a group of spectral lines having Doodson numbers where the first three digits are identical [*Ray*, 2007]) are split by the nodal and perigean modulations, generating additional lines whose frequencies differ from the primary frequencies by one or two (i.e., subharmonics) cycles per 18.61 or 8.85 years, respectively. When tidal records with durations approaching or exceeding the 18.61 year nodal period are analyzed, it is possible to calculate the amplitude and phases of these "satellites" of the major constituents [e.g., *Foreman and Neufeld*, 1991; *Cherniawsky et al.*, 2010]. Hence, when the individual tidal constituents are summed, the interannual tidal modulations are included directly in the tidal predictions. However, tidal

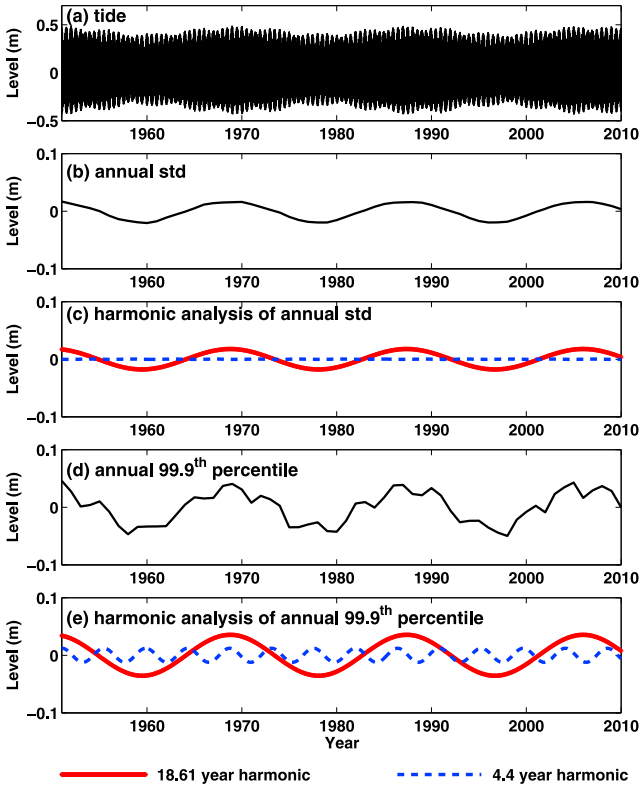

Figure 2. (a) The tide. (b) Annual standard deviation of the tide. (c) The 18.61 (solid) and 4.4 (dotted) year harmonic signals calculated from the annual standard deviation time series. (d) The annual 99.9th percentile. (e) The 18.61 and 4.4 year harmonic signals calculated from the 99.9th percentile time series for the grid node nearest to Fremantle, Western Australia. Note that the standard deviation and percentile time series have been plotted with their means removed.

analyses are typically performed using only a year or two of tide gauge observations. When only a few years of records are analyzed, only the frequencies that differ by at least one multiple of the third harmonic (h) can be included in the tidal analysis [*Cherniawsky et al.*, 2010]. Hence, the influence of the nodal and perigean modulations must be represented indirectly in some way [*Pugh*, 2004]. Traditionally, these effects have been handled using small adjustment factors f (amplitude amplification factor) and u (angle), which are usually assumed to vary in the same way as gravitational potential varies and are estimated from astronomical parameters [see *Cartwright and Tayler*, 1971; *Cartwright and Edden*, 1973; and *Pugh*, 1987, Table 4:3]. The factors f and u are often called nodal factors or nodal modulation corrections. However, the term "nodal modulation," as *Foreman* [1977] points out, is a misnomer. It, and the factors f and u, were first used before the advent of modern computers to designate corrections for the Moon's nodal progression that were not incorporated into calculations of the astronomical argument for the main constituents. The term "satellite modulation" is more appropriate now (and is used throughout this paper) because the correction accounts for not only the contribution of the lunar node but also the lunar and solar perigee effects.

[15] The factors that determine f and u for the major lunar constituents are given in Table 1. For M_2 and N_2, the maximum equilibrium nodal variation is 3.7%. For K_2, the maximum variation is 28.6%. O_1 and Q_1 vary by 18.7% of the mean amplitude, and K_1 varies by 11.5%. For the solar constituents S_2 and P_1, f and u are 1.0 and 0.0. The minor constituents, M_1 and L_2, are also affected by the 8.85 year cycle of lunar perigee. For these constituents, f and u are more complex and involve terms with both N and p [*Pugh*, 1987].

[16] With recent advances in global ocean tidal models, altimetry missions (e.g., TOPEX/Poseidon, Jason-1, and Jason-2), and assimilation methods, accurate maps of the main tidal constituents are now available on a global scale (see *Andersen* [1995] and *Shum et al.* [1997] for reviews). Using these major constituents, the minor constituents that can be inferred from them [*Godwin*, 1972], and satellite modulation corrections based on equilibrium tide expectations (described above), predictions of the tide, with interannual tidal modulations included, can be made for locations around the world. From these tidal predictions, the influence of the 18.61 year lunar nodal cycle and 8.85 year cycle of lunar perigee on high tidal levels can be examined on a global scale. This is the basis of the method used in this current study.

3. Methodology

[17] In this paper, tidal constituents from the TPXO7.2 global tidal model are used, with satellite modulation corrections based on equilibrium tide expectations, to predict multidecadal time series of tides. TPXO7.2 best fits (in a least squares sense) the Laplace tidal equations and along-track averaged data from the TOPEX/Poseidon and Jason altimetry missions obtained with Oregon State University Tidal Inversion Software (OTIS). The tides are provided for eight primary (M_2, S_2, N_2, K_2, K_1, O_1, P_1, and Q_1), two long-period (M_f and M_m), and three nonlinear (M_4, MS_4, and MN_4) harmonic constituents on a one-quarter degree resolution full global grid (see *Egbert et al.* [1994] and *Egbert and Erofeeva* [2002] for more details). The amplitudes of the eight primary and two long-period constituents are shown in Figure 1a.

[18] The harmonic constituents were downloaded from the OTIS Web site (http://volkov.oce.orst.edu/tides/), and the tide was predicted (from these constituents) using the Tidal Model Driver (TMD) MATLAB toolbox created by scientists at Earth Space Research (http://polaris.esr.org/ptm_index.html). TMD includes standard satellite modulation corrections based on equilibrium tide expectations and also includes 16 other minor constituents in the tidal prediction ($2Q_1$, $sigma_1$, rho_1, M_1, chi_1, pi_1, phi_1, $theta_1$, J_1, OO_1, $2N_2$, mu_2, nu_2, $lambda_2$, L_2, and t_2). The amplitude and phase of these minor constituents are inferred from the eight major constituents. The tide was predicted every hour for a 60 year period (January 1951 to December 2010) for each ocean grid node on a one-quarter degree resolution full global grid (1400 × 721 grid cells). (It is important to note that this method does not consider the nodal tide, which influences mean sea levels (see *Pugh* [1987] for details). However, as the nodal tide is small (theoretically <0.02 m), the influence

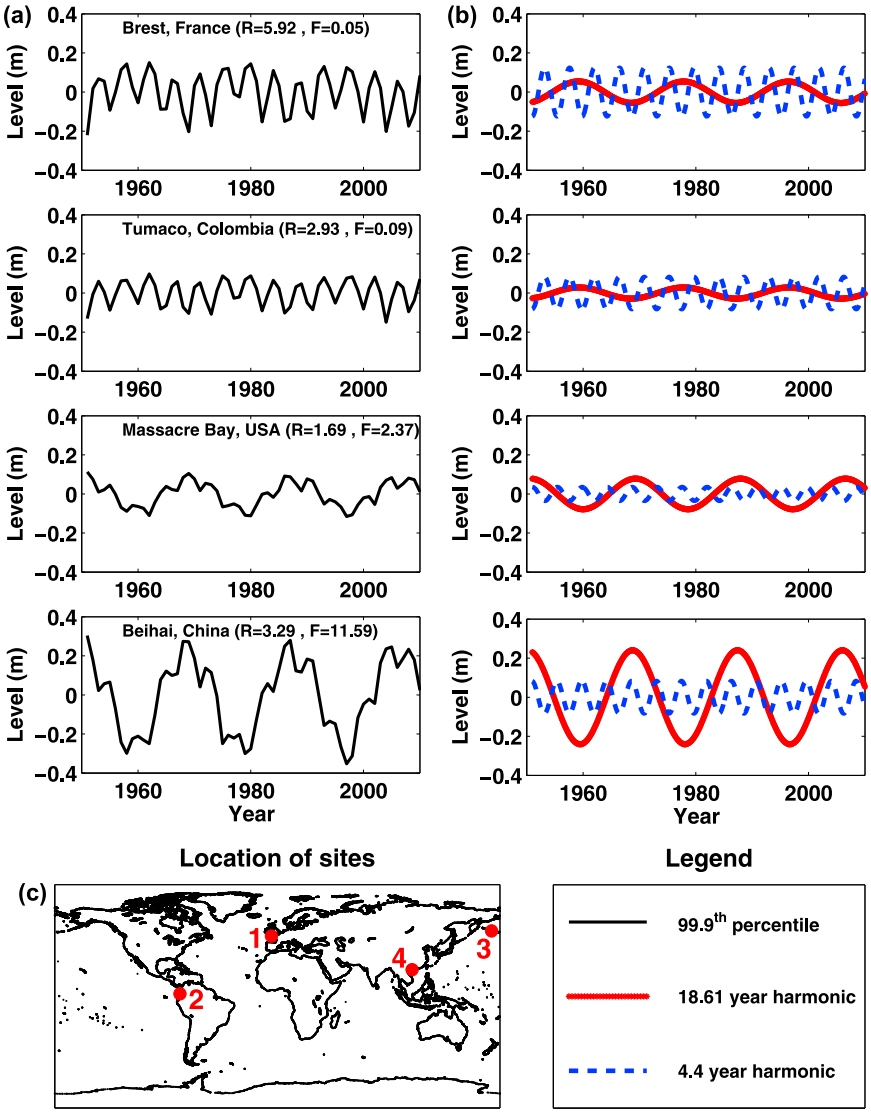

Figure 3. (a) The annual 99.9th percentile. (b) The 18.61 and 4.4 year harmonic signals calculated from the 99.9th percentile time series for four sites around the world. (c) The locations of the four sites are shown. Note that *R* is tidal range and *F* is form factor; these time series have been plotted with their means removed.

on high tidal levels is also likely to be small and hence will not significantly impact the results.)

[19] Two robust methods were used to determine the influence of tidal modulations on high tidal levels across the globe. First, the standard deviation of the 60 year tidal time series was calculated for each calendar year at each ocean grid node following *Pugh* [2004], *Araújo and Pugh* [2008], and *Eliot* [2010]. Second, the hourly tidal values for each calendar year were ordered in terms of height and used to calculate time series of various percentile levels. The percentile time series analysis method is described in detail by *Woodworth and Blackman* [2004] and has been used extensively in sea level research. As the aim of this study is to determine the contribution of tidal modulations to high tidal levels, we focus on the 99.9th percentile, which is the height below which the tide remains for 99.9% of the observations. This corresponds approximately to the level of the eight highest hourly sea level values in a year. However, to consider the sensitivity of the results to the percentile level chosen, time series for an additional 19 percentile levels, ranging from median to annual maximum (50th, 60th, 70th, 80th, 90th, 95th, 96th, 97th, 98th, 99th, 99.1th, 99.2th, 99.3th, 99.4th, 99.5th, 99.6th, 99.7th, 99.8th, and 100th), were also calculated for each ocean grid node (using the 60 year time series described above).

[20] The amplitude and phase of the tidal modulations and their subharmonics were estimated from both the annual standard deviations and each percentile time series using harmonic analysis fitted to 18.61, 9.305, 8.85, and 4.425 year sinusoidal signals. The amplitudes of the 9.305 and 8.85 year cycles were typically more than an order of magnitude smaller than that of the 18.61 and 4.425 year cycles, respectively, and hence are not considered further. The procedure for the grid node nearest to Fremantle, Western Australia (32°, 115°), can be seen in Figure 2.

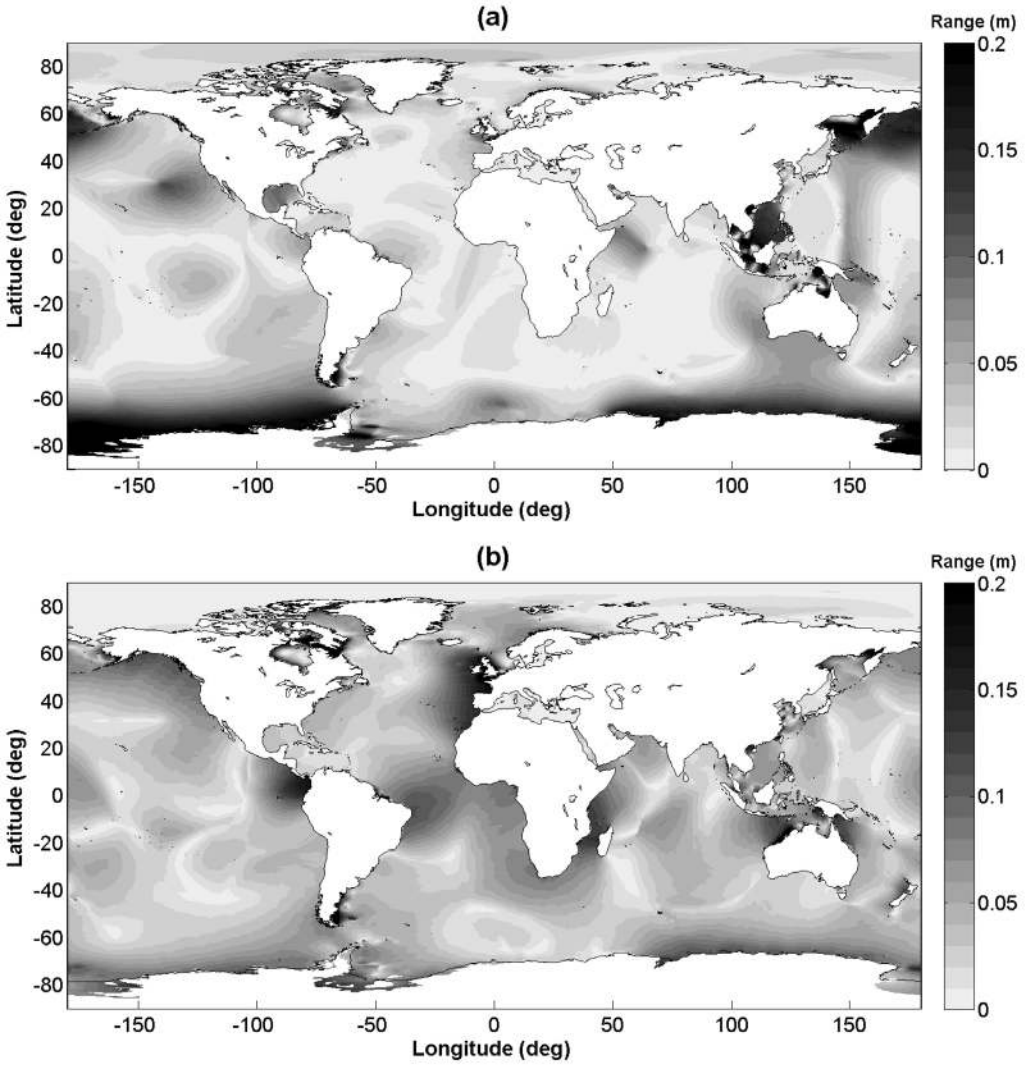

Figure 4. (a) Range of the 18.61 year modulation in the 99.9th percentile tidal level. (b) Range of the 4.4 year modulation in the 99.9th percentile tidal level.

[21] Tests were undertaken to assess the sensitivity of the method to the length and timing of the tidal time series. The tide was calculated for the 101 year period from 1910 to 2010 for four sites, the locations of which are shown in Figure 3. These four sites were chosen to (1) sample a range of different tidal conditions (i.e., the tides at sites 1 and 2 are semidiurnal in form, at site 3 they are mixed but mainly diurnal in form, and at site 4 they are strongly diurnal) and (2) illustrate different characteristics of the interannual tidal modulations based on the results of the global assessment (i.e., sites 1 and 2 are dominated by the 4.4 year cycle; sites 3 and 4 are dominated by the 18.61 year cycle). Annual standard deviation and 99.9th percentile time series were derived for each year of the 100 year time series. Harmonic analysis for the four cycles was undertaken for record lengths of 18, 19, and up to 100 years, with the starting date varied to cover the full range of the time series (e.g., when considering 31 year lengths, the subsets 1910–1940, 1911–1941, and so on up to 1980–2010 were analyzed). It was found (results not shown) that when record lengths of at least three complete nodal cycles (i.e., about 56 years) were used, the amplitude of the four cycles varied by less than 1 cm, irrespective of the start and end dates of the tidal record, justifying the use of a 60 year time series for the main analysis.

[22] The spatial variations in the range (i.e., twice amplitude) and phase of the 18.61 and 4.4 year modulations in high tidal levels are related to the global distribution of the main tidal constituents and the form and range of the tide. The tidal form factor and range have been calculated at each of the ocean grid nodes using the TPXO7.2 global database of tidal constituents. The form factor (F) has been derived from the main harmonic constituent amplitudes (H) using the following equation:

$$F = \left(\frac{H_{K_1} + H_{O_1}}{H_{M_2} + H_{S_2}} \right).$$

The tides may be roughly classified as [*Pugh*, 2004] F = 0–0.25 for the semidiurnal form; F = 0.25–1.50 for the mixed,

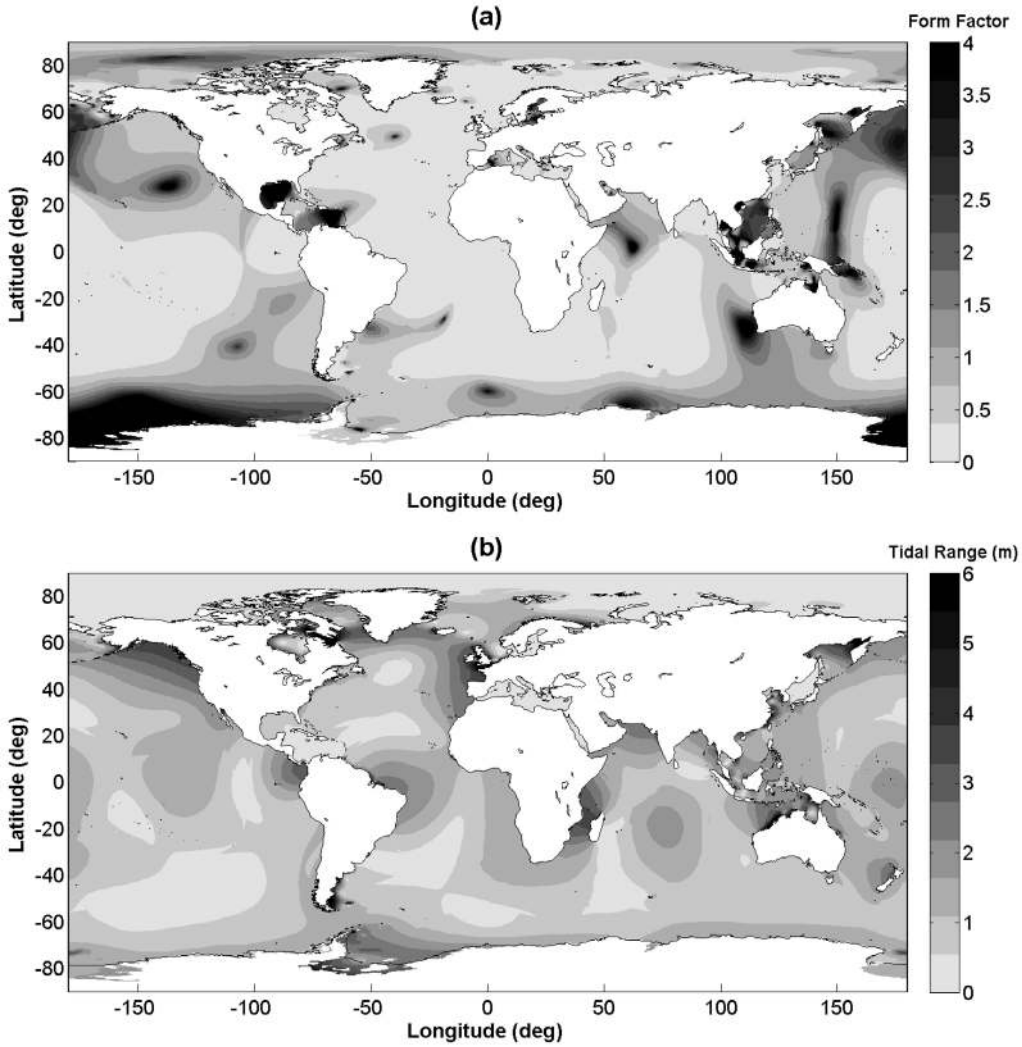

Figure 5. (a) Tidal form factor. (b) Tidal range.

mainly semidiurnal form; F = 1.50–3.00 for the mixed, mainly diurnal form; and $F > 3.00$ for the diurnal form.

[23] For semidiurnal locations ($F < 0.25$), the tidal range has been estimated as the difference between mean high water springs (MHWS) and mean low water springs (MLWS), calculated by the following equations:

$$\mathrm{MHWS} = H_{\mathrm{M}_2} + H_{\mathrm{S}_2}$$

$$\mathrm{MLWS} = -(H_{\mathrm{M}_2} + H_{\mathrm{S}_2}).$$

For mixed and diurnal locations ($F > 0.25$), the tidal range has been estimated as the difference between mean higher high water (MHHW) and mean lower low water (MLLW), calculated by the following equations:

$$\mathrm{MHHW} = H_{\mathrm{M}_2} + H_{\mathrm{K}_1} + H_{\mathrm{O}_1}$$

$$\mathrm{MLLW} = -(H_{\mathrm{M}_2} + H_{\mathrm{K}_1} + H_{\mathrm{O}_1}).$$

The tidal range (R) is typically classified as R = 0–2 m for microtidal, R = 2–4 m for mesotidal, and R = >4 m for macrotidal.

4. Results

4.1. Range of Tidal Modulations

[24] Figure 4 shows the ranges of the 18.61 and 4.4 year modulations in the 99.9th percentile tidal level on a global scale. The range of the 18.61 year modulation (Figure 4a) is largest (between 0.5 and 0.8 m) in the Gulf of Tonkin (in the South China Sea), in the Shelikhov Gulf (in the Sea of Okhotsk), along the southwestern coast of New Guinea (in the Arafura Sea), and in the Ross Sea. The range of the 4.4 year modulation (Figure 4b) is largest (between 0.3 and 0.6 m) in the eastern part of the Bering Sea, in the Hudson Strait, in the Gulf of Panama, on the Patagonian Shelf, in the Irish Sea, in the Bristol Channel and English Channel, at the entrance to the White Sea, on the northwest Australian Shelf, and in the Shelikhov Gulf.

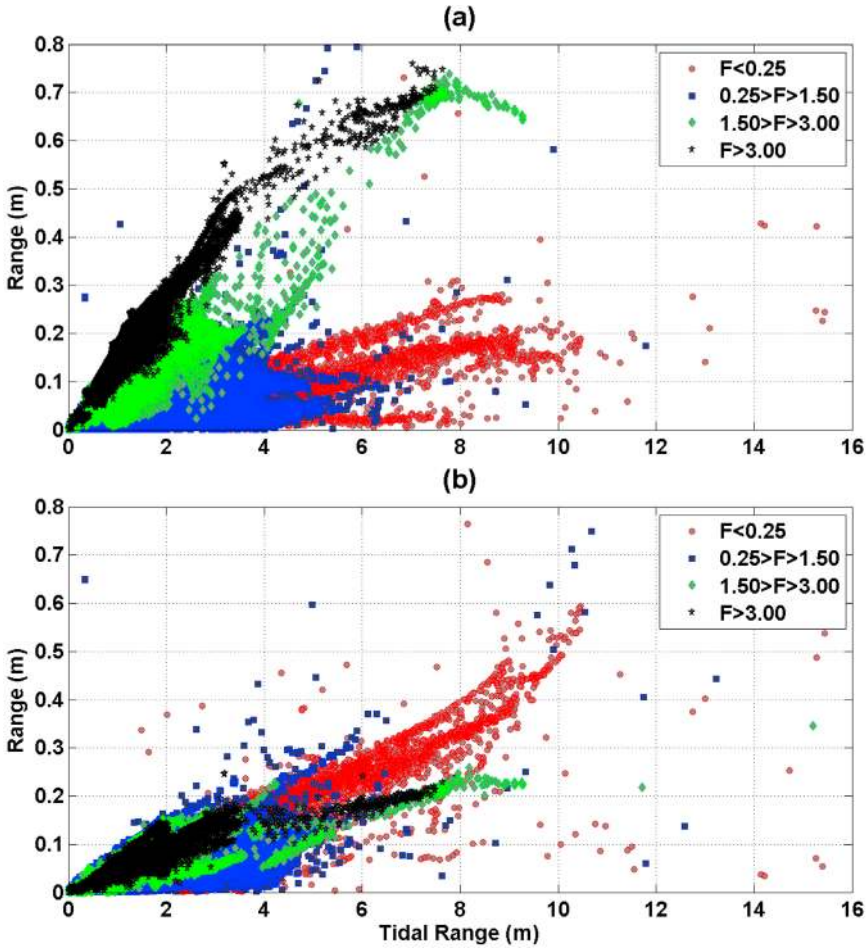

Figure 6. Ranges of the (a) 18.61 and (b) 4.4 year modulation in the 99.9th percentile tidal level plotted against the tidal range.

[25] Spatial variations in the range of the 18.61 year modulation (Figure 4a) are related to the global distribution of the main tidal constituents (Figure 1a). However, it is the amplitude of the tidal constituents multiplied by the relevant satellite modulation corrections that determines the variations in the nodal modulations and not just the amplitude of the tidal constituents. Figure 1b shows the amplitudes of the eight primary and two long-period tidal constituents multiplied by the relevant satellite modulation corrections listed in Table 1. The multiplied constituents M_2, K_2, K_1, and O_1 are clearly dominant (hereafter we refer to these as M_{2n}, K_{2n}, K_{1n}, and O_{1n}, and likewise for the other constituents). Although the amplitude of K_2 is considerably smaller than that of M_2 (Figure 1a), the amplitude of K_{2n} is similar in magnitude to M_{2n} (Figure 1b). This is because the satellite modulation correction is much larger: 28.6% for K_2 as opposed to 3.7% for M_2. The amplitude of O_1 is typically smaller than the amplitude of K_1, but the amplitudes of O_{1n} and K_{1n} are similar in magnitude, given that K_1 is multiplied by 11.5% while O_1 is multiplied by 18.7%. The amplitudes of S_{2n} and P_{1n} are zero because they are solar constituents. The amplitudes of N_{2n}, Q_{1n}, M_{fn}, and M_{mn} are relatively small (typically <1 cm) because the amplitudes of N_2, Q_1, M_f, and M_m are small in the first place.

[26] In relating the spatial variations in the range of the 18.61 year modulation to the distribution of the amplitude of the dominant constituents M_{2n}, K_{2n}, K_{1n}, and O_{1n}, the sign of the satellite modulation terms (listed in Table 1) also needs to be considered. The amplitudes of K_{2n}, K_{1n}, and O_{1n} are largest when $N = 0°$ (because of the positive sign), whereas M_{2n} is largest when $N = 180°$ (because of the negative sign). Hence, when the modulated tidal constituents are summed, K_{2n}, K_{1n}, and O_{1n} will act to reduce the influence of M_{2n} on high tidal levels.

[27] The opposing phase and differences in satellite modulation corrections help to explain spatial variation of the 18.61 year modulation range (Figure 4a) in terms of the amplitudes of M_{2n}, K_{2n}, K_{1n}, and O_{1n} (Figure 1b). For areas where M_{2n} is large and the other contributing constituents are small, or vice versa, the nodal modulation is relatively large and therefore may occur at locations where the tide is either diurnal or semidiurnal in form. The large nodal modulations in the Gulf of Mexico, western and northern Pacific Ocean, and Southern Ocean are a result of the large amplitudes of K_{1n} and O_{1n} in these regions. These areas are either mixed or diurnal in form (Figure 5a). The large nodal modulations in the Hudson Strait, on the Patagonian Shelf, in the Bristol and English channels, and at the entrance to

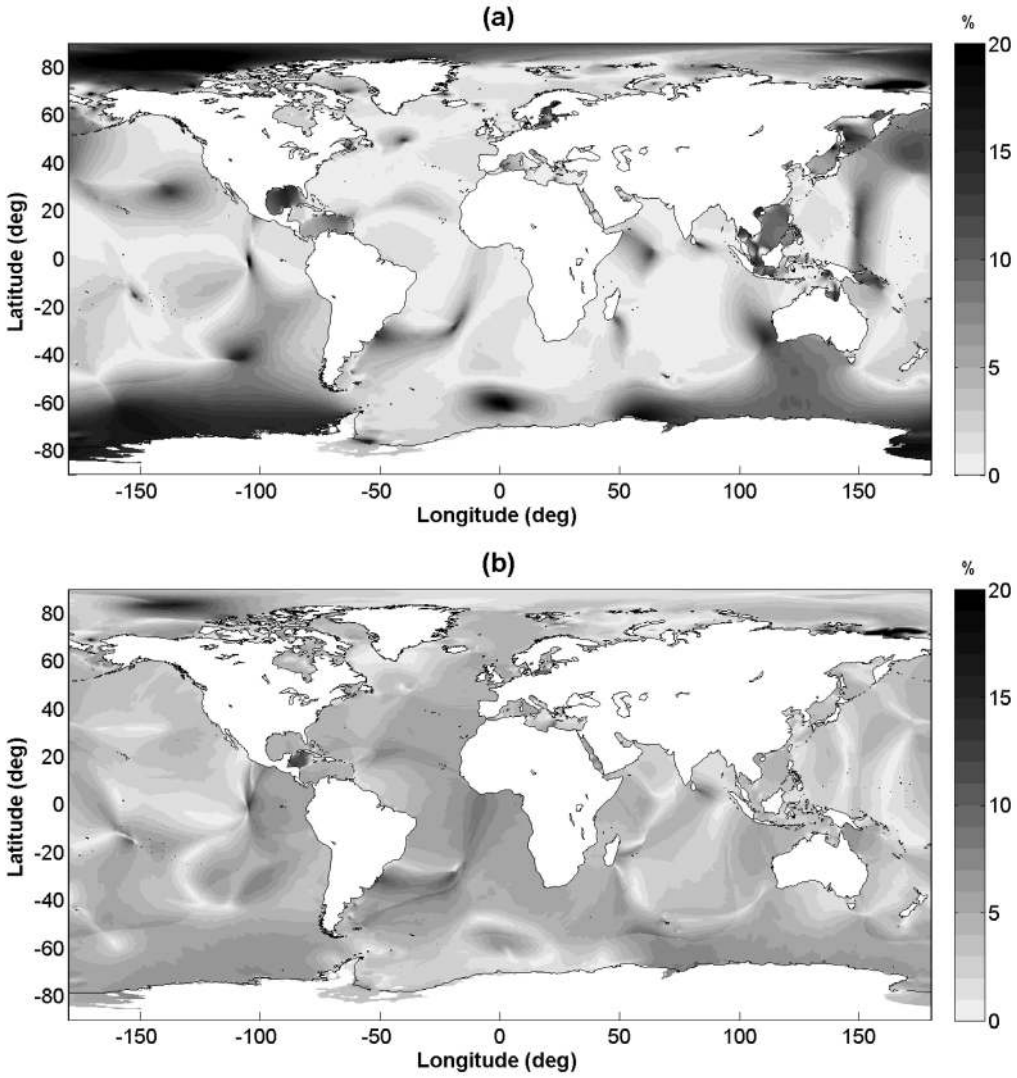

Figure 7. Ranges of the (a) 18.61 and (b) 4.4 year modulation in the 99.9th percentile tidal level expressed as a percentage of the tidal range.

the White Sea are a result of the large amplitude of M_{2n} in these regions. These areas are semidiurnal in form (Figure 5a) and have very large tidal ranges (Figure 5b).

[28] For areas where there is less difference in scale between M_{2n} and the other contributing constituents, the opposing phase of the modulations causes a reduction of the 18.61 year range. There are several regions where the amplitude of M_{2n} is large but the range of the nodal modulations is small, e.g., in the Gulf of Alaska, in the Mozambique Channel, and offshore of Panama, Colombia, and Ecuador. In the Gulf of Alaska, the nodal modulations are small as the influence of M_{2n} is reduced by K_{1n} and O_{1n}, which are also large in this region. Offshore of Panama, Colombia, and Ecuador and in the Mozambique Channel, the large amplitude of M_{2n} is reduced by K_{2n}, the amplitude of which is also large in this region. The band of large nodal modulations, extending from the Sea of Okhutsk to the Solomon Sea, can be seen to relate to the large amplitudes of K_{1n} and O_{1n} and the small amplitude of M_{2n} in this area. On either side of this band, the amplitude of M_{2n} is larger and reduces the influence of K_{1n} and O_{1n} in these areas.

[29] The spatial variations in the range of the 4.4 year modulation (Figure 4b) cannot be expounded in the same way as the nodal variations, described above, can. The M_1 and L_2 constituents have a perigean modulation, but the satellite modulation corrections are more complex, involving terms with both N and p, and hence, they cannot simply be factored, as is done in Figure 1b. The amplitudes of the M_1 and L_2 constituents (which are inferred in TMD from the primary constituents) are much smaller than the amplitudes of M_{2n}, K_{2n}, K_{1n}, and O_{1n} and alone cannot account for the large range of the 4.4 year modulation observed in Figure 4b. However, the addition of nodal-modulated M_2, N_2, and K_2 constituents and/or the addition of nodal-modulated K_1, O_1, and Q_1 constituents results indirectly in a 4.4 year modulation. It appears that it is this mechanism that accounts for the majority of the observed 4.4 year modulation. Interestingly, the spatial variations in the range of the 4.4 year

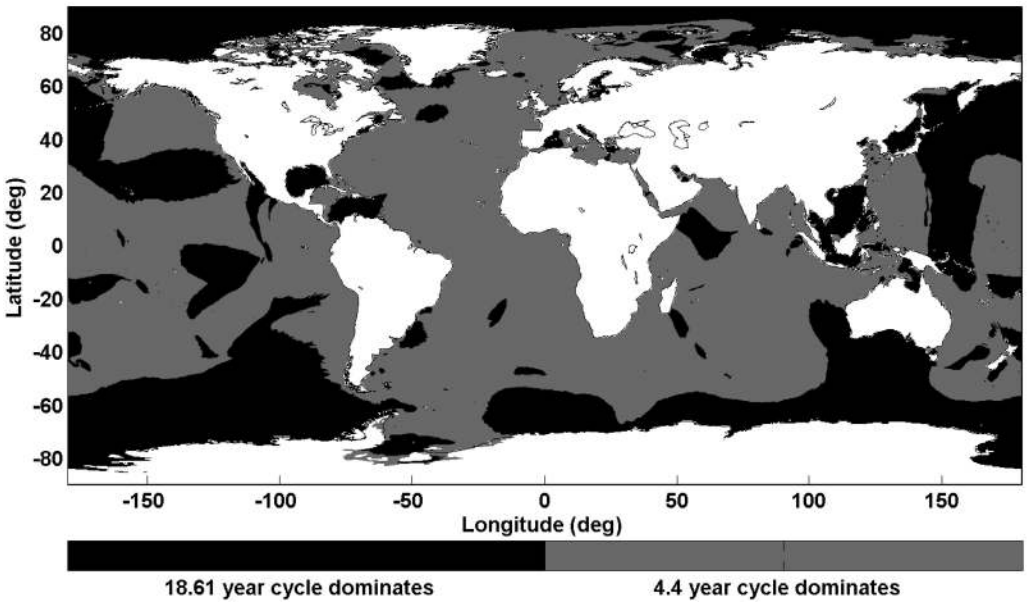

Figure 8. Regions of the world's oceans where the range of the 18.61 year modulation in the 99.9th percentile tidal level is larger than that of the 4.4 year modulation and vice versa.

modulation can be seen to relate, to a large degree, to the range of the tide (Figure 5b).

[30] Figures 6a and 6b show the ranges of the 18.61 and 4.4 year modulation in the 99.9th percentile level plotted against the tidal range, respectively. The plots distinguish between grid cells where the tide is semidiurnal, mixed but mainly semidiurnal, mixed but mainly diurnal, or diurnal in form. The vast majority of the data points fit in distinct bands. The few points that are scattered away from these bands all lie near the coast in narrow channels or inlets. This may result from the inaccuracy of the relatively coarse global tidal model for coastal locations with complex topography.

[31] The range of the 18.61 year modulation generally increases with tidal range (Figure 6a). However, the range of the nodal modulation typically increases more with tidal range for locations dominated by diurnal tides as compared to locations dominated by semidiurnal tides. The average slope of the curve is about 3 to 5 times steeper for the locations dominated by diurnal tides as compared to the locations dominated by semidiurnal tides. This is expected, given that the satellite modulation corrections for K_1 and O_1 are about 3 and 5 times larger, respectively, than the correction for M_2 (Table 1). The nodal modulation is largest (between 0.5 and 0.8 m) in regions dominated by diurnal tides with tidal ranges of >4 m (Figure 6a).

[32] The range of the 4.4 year modulation also increases with tidal range (Figure 6b), but the differences between the various form factor bands are not as pronounced as with the nodal modulation (Figure 6a). The range of the 4.4 year modulation increases more at locations with larger semidiurnal tides, which is the opposite of the case with the nodal modulation. The 4.4 year modulation is largest (between 0.3 and 0.6 m) in regions dominated by semidiurnal tides where the tidal range is >6 m.

[33] From a coastal flooding perspective, it is interesting to consider the range of the tidal modulations as a percentage of the tidal range at a given site. At two different sites, the range of the 18.61 or 4.4 year modulations might be around 10 cm; however, the influence of the interannual tidal modulations is likely to be more significant at the site with the smaller tidal range, as *Eliot* [2010] found for Western Australia. Figures 7a and 7b show the ranges of the 18.61 and 4.4 year modulations, respectively, expressed as a percentage of the tidal range. Around southwest Australia, in the Gulf of Mexico, and around southern England, the range of the 18.61 year modulation is of similar magnitude: about 10 cm (Figure 4a). However, the range of the 18.61 year modulation is about 17% of the tidal range around southwest Australia and in the Gulf of Mexico but is less than 5% of the tidal range around southern England (Figure 7a). The range of the 18.61 year modulation is the largest percentage of the tidal range mainly in areas where the tide is strongly diurnal (Figure 5a). The range of the 4.4 year modulation is at least 5% of the tidal range in a large proportion of the world's oceans (Figure 7b). In the Caribbean Sea, the range of the 4.4 year modulation is over 15% of the tidal range.

[34] It is also important to determine which of the two cycles is more dominant in high tidal levels at a given location, which would allow coastal managers to predict whether periods of enhanced risk of coastal flooding are likely every 18.61 or 4.4 year. Figure 8 shows the regions where the range of 18.61 year modulation is larger than the range of the 4.4 year modulation in high tidal levels, and vice versa. The spatial distribution closely resembles that of the tidal form factor (Figure 5a). The lunar nodal modulation dominates over the 4.4 year modulation in regions where the tide is mixed or diurnal in form, whereas the 4.4 year modulation dominates high tidal levels in regions where the tide is semidiurnal in form. The patterns observed for

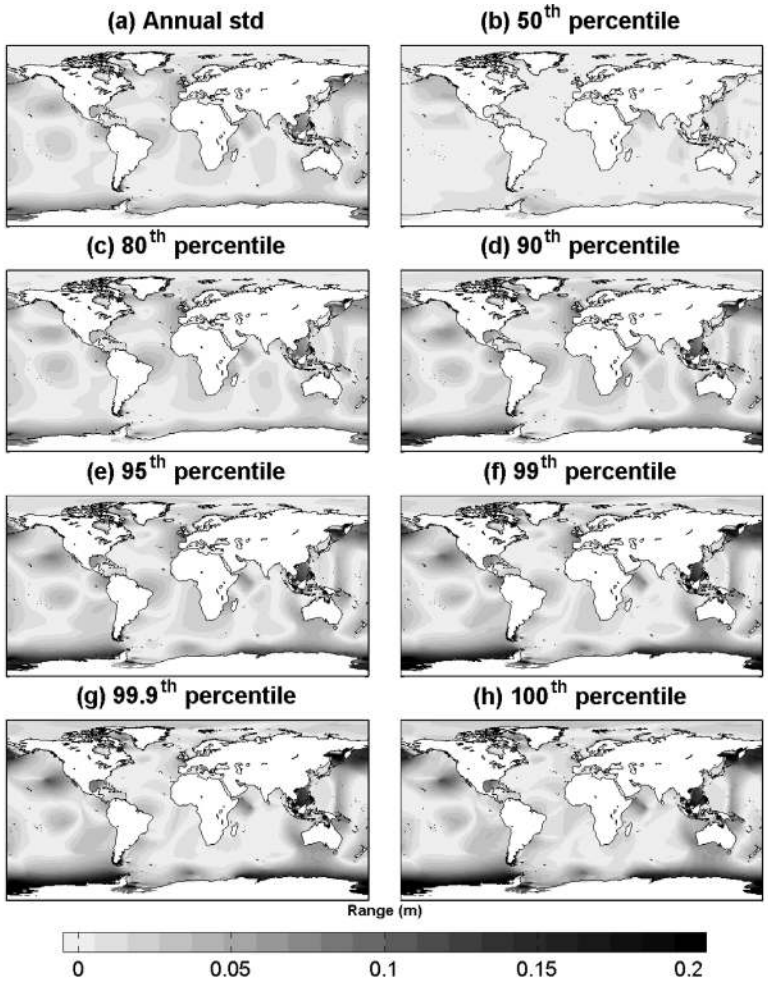

Figure 9. (a–h) Range of the 18.61 year modulation in the standard deviation time series and for various percentile tidal levels.

Western Australia are consistent with those observed by *Eliot* [2010], showing that the nodal modulation dominates high tidal levels in the southwest (diurnal) region and that the 4.4 year modulation dominates high levels in the northwest (semidiurnal) region. An analysis of the data reveals that the 4.4 year modulation tends to dominate in regions where the form factor is <~0.6.

[35] Up to this point, only the ranges of the interannual tidal modulations in the 99.9th percentile tidal level have been considered. The ranges of the 18.61 and 4.4 year modulations were also calculated for the annual standard deviation time series and for an additional 19 percentile levels. Figures 9 and 10 show the ranges of the 18.61 and 4.4 year modulations, respectively, calculated from the standard deviation time series and for a selection of percentile levels. The ranges of the two modulations are sensitive to the percentile level chosen, particularly for the 4.4 year modulation, but the relative spatial distributions are generally similar. The range in the annual tidal standard deviation is smaller than that calculated from the 99.9th tidal percentile, but the global spatial distributions are similar. The range of the 4.4 year modulation is reduced, more than that of the 18.61 year modulation, when lower percentile levels are considered. The range of the 4.4 year modulation is negligible in the annual standard deviation time series, allowing focus on the nodal cycle. *Eliot* [2010] used time series of monthly percentile levels at two tide gauge sites around Western Australia to explain the inability of annual standard deviations to successfully identify the influence of lunar perigee. When the lunar perigean cycle acts to enhance equinoctial tides, there is also a corresponding diminishing of high tidal levels around the time of the solstices. As standard deviations equally weight both phases, the annual standard deviation is virtually constant.

4.2. Phase of Tidal Modulations

[36] The 18.61 year lunar nodal precession has a large effect on the Moon's declination, which in turn has a large effect on the character of lunar tidal forcing. When $N = 0°$, the Moon's declination is at a maximum (28°36′), which tends to maximize diurnal forces at the expense of semidiurnal forces [*Ray*, 2007]. Hence, nodal modulation of diurnal tides is at a maximum when $N = 0°$, which last occurred in 2006, whereas when $N = 180°$, the Moon's declination is at a minimum (18°18′), which tends to maximize semidiurnal forces at the expense of diurnal forces.

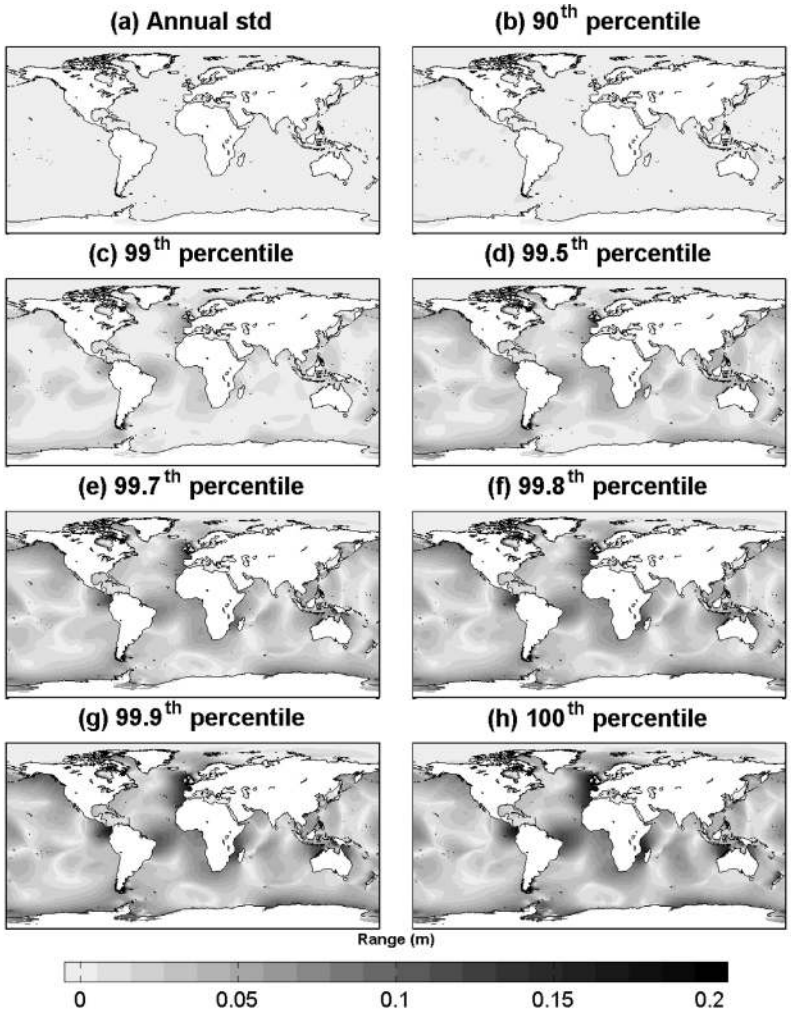

Figure 10. (a–h) Range of the 4.4 year modulation in the standard deviation time series and for various percentile tidal levels.

Hence, the nodal modulation of semidiurnal tides is at a maximum when N = 180°, which last occurred in 1997. Therefore, the nodal modulation in high tidal levels will have one of two phases at a given location depending on whether that site is dominated by semidiurnal or diurnal tides. This can be clearly seen in Figure 3. At sites 1 and 2 (Figures 3a and 3b), where the tide is semidiurnal in form, the nodal modulation last peaked in 1997, whereas at sites 3 and 4 (Figures 3c and 3d), where the tide is mixed or diurnal in form, the nodal modulation last peaked in 2006.

[37] Figure 11 shows the phase (in degrees, with the origin of time taken as midnight on 1 June 2006 at the Greenwich meridian) of the 18.61 year modulation calculated by harmonic analysis of the annual tidal standard deviation time series. As expected, two phases are evident. One phase (0°) corresponds with the point when the nodal tidal modulation last peaked in 2006 and correlates with maximum lunar declination (i.e., N = 0°), whereas the other phase (180°) corresponds with the point when the nodal tidal modulation last peaked in 1997 and correlates with minimum lunar declination (i.e., N = 180°). An analysis of the data reveals that at the locations where the nodal cycle last peaked in 1997, the form factor is <~0.6, consistent with results described in section 4.1.

[38] The results shown in Figure 11 are consistent with those found by *Eliot* [2010] for Western Australia, showing that the nodal cycle is out of phase between the southern (diurnal) and northern (semidiurnal) regions. The results are also consistent with those of *Marmer* [1951] and *Kaye and Stuckey* [1973], who identified that the nodal tidal modulations were out of phase between the East Coast of the United States (semidiurnal) and in the Gulf of Mexico (diurnal).

[39] Examination of Figure 3 shows that the 4.4 year modulation in high tidal levels also has two phases that, like the nodal modulation, appear to be related to the form of the tide. However, considering the nature of the cycle of lunar perigee (described in section 2), it is not clear why this should be the case. It could be due to the fact, as outlined above, that the majority of the 4.4 year modulation appears to arise indirectly from either the addition of nodal-modulated M_2, N_2, and K_2 constituents or the addition of nodal-modulated K_1, O_1, and Q_1 constituents, rather than directly through the M_1 and L_2 constituents. Sensitivity tests (results not shown)

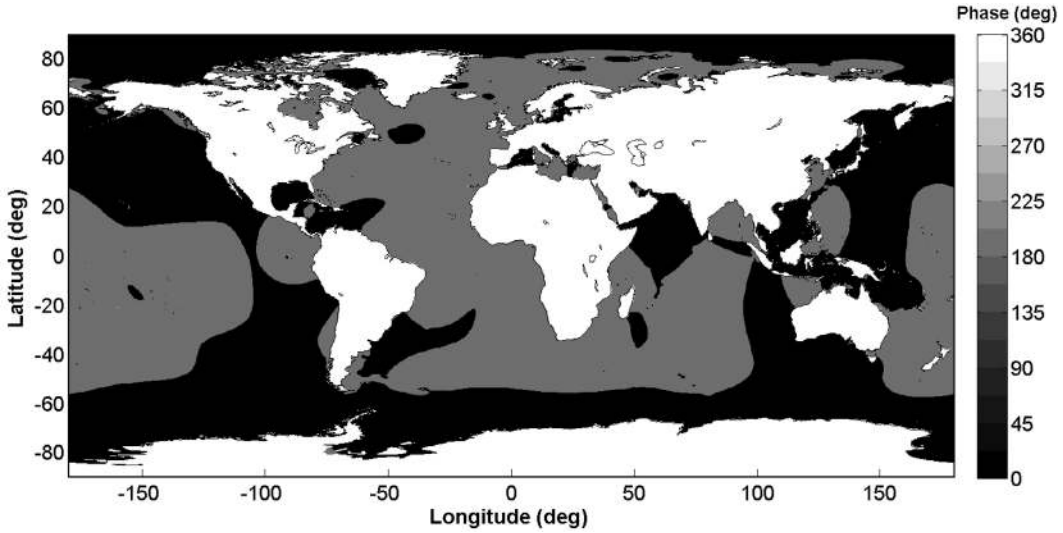

Figure 11. Phase (in degrees with the origin of time taken as midnight on 1 June 2006 at the Greenwich meridian) of the 18.61 year modulation in the annual tidal standard deviation.

show that the addition of nodal-modulated M_2, N_2, and K_2 constituents produce a 4.4 year cycle that is 180° out of phase of that produced by the addition of nodal-modulated K_1, O_1, and Q_1 constituents. The global distribution of the phase of the 4.4 year modulation is similar to that observed in the nodal modulation (Figure 11).

5. Discussion

[40] This paper has used modeled tides to estimate the contribution of the 18.61 year lunar nodal cycle and the 4.4 year cycle of perigean influences to high tidal levels on a global scale. The results show that the lunar nodal modulation can have a range of up to about 0.8 m in certain locations, while the range of the 4.4 year modulation can be up to about 0.6 m in certain areas. The regions where the nodal modulations are largest are in areas with large diurnal tides. In the literature [e.g., *Jeuken et al.*, 2003; *Gratiot et al.*, 2008], areas with large nodal influence have tended to be linked to regions with large semidiurnal tides (i.e., where the M_2 tidal constituent is large), disregarding nodal influences in diurnal regions. *Woodworth et al.* [2005] identified that many studies also mistakenly ignore the role of diurnal tides in discussions of tidal asymmetry.

[41] This current study has also examined the phase of the tidal modulations, highlighting that there are two phases in both the 18.61 and the 4.4 year modulations in high tidal levels, which are dependent on the form of the tide. The phases of the interannual tidal modulations are important from a coastal flooding perspective, and yet, surprisingly, there are few discussions of this in the literature.

[42] In their study relating the nodal cycle to coastal erosion, *Gratiot et al.* [2008, Figure 3] estimated the amplitude of the nodal modulation on a global scale by multiplying mean high water level (calculated from a global map of tidal amplitude proposed by *Simon* [2007]) by 3.7%. Gratiot et al. used this to estimate regions of the world's coastlines that could experience significant coastal erosion over the next decade. Our estimates are reasonably consistent with those of *Gratiot et al.* [2008] in some regions with large semidiurnal tides (e.g., in the Hudson Strait and Bay of Fundy, on the Patagonian Shelf, and in the Bristol and English channels). This is expected because the M_2 tidal constituent dominates in these regions. However, the approach of multiplying high water level by the M_2 satellite modulation correction (3.7%) significantly overestimates the amplitude of the nodal modulation around northwest Australia, in the East China Sea, and in the Bass Strait, where the amplitudes of M_2, K_1, and O_1 are all relatively large. Furthermore, this approach also does not account for the areas where the nodal modulations are largest (i.e., diurnal areas with large tidal ranges such as along the southwestern coast of New Guinea). Importantly, the estimates of *Gratiot et al.* [2008] did not account for the phase difference between diurnal and semidiurnal regions. While regions with semidiurnal tides may experience significant coastal erosion over the next decade, regions with mixed and diurnal tides will see a reduction in coastal erosion over the next decade.

[43] In undertaking this study, two main assumptions were made: (1) the modeled tidal constituents are accurate, and (2) the real nodal and perigean tidal satellite constituents conform in the same way as do their equilibrium counterparts. In regard to the first point, we have used the TPXO7.2 global tidal model, which is one of over 20 global ocean tide models that have been developed over the past two decades. *Shum et al.* [1997] assessed the accuracy of 10 global tidal models (including an earlier version of the TPXO model). In the deep ocean, the models were shown to be very accurate and agreed to within 2–3 cm. However, larger differences were identified in shallow water regions. It would be interesting, particularly with a focus on shallow water regions, to repeat the exercise undertaken in this current study using tidal constituents for a range of global tidal models and also from higher-resolution regional tidal models.

[44] In regard to the second point, several studies have compared the observed tidal nodal modulations with their corresponding nodal equilibrium tidal constituents and have shown that differences do occur at some locations (see *Cherniawsky et al.* [2010] and *Shaw and Tsimplis* [2010] for a review). However, as these previous studies focus on modulations in individual tidal constituents, it is difficult to determine the combined impact these differences have on modulations at high tidal levels. Considering that the differences found for individual tidal constituents are relatively small, it is likely that any changes to the interannual tidal modulations would also be small.

[45] Recently, *Cherniawsky et al.* [2010] undertook harmonic analyses of 16 year long time series of altimeter data for the Pacific and western Atlantic oceans and directly estimated the amplitude of the nodal satellites M_{2n}, K_{2n}, K_{1n}, O_{1n}, and Q_{1n} from their parent constituents M_2, K_2, K_1, O_1, and Q_1. A visual comparison between their measured results (presented by *Cherniawsky et al.* [2010, Figures 1–5] and the modeled ones (presented in Figure 1b) suggested reasonable agreement. This implies both that the TPXO7.2 modeled tidal constituents are reasonably accurate and that the real nodal satellite constituents conform in a way similar to that of their equilibrium counterparts.

[46] This paper has analyzed modeled tides, and there is a need to compare the results with observational data. Recently, *Menéndez and Woodworth* [2010] examined the occurrence of extreme high water levels using the Global Extreme Sea Level Analysis (GESLA) quasi-global tide gauge data set compiled by staff at the Antarctic Climate and Ecosystems Cooperative Research Centre (Australia) and the National Oceanography Centre (Liverpool, U. K.). Using nonstationary extreme value analysis based on monthly maxima, they estimated the amplitudes of the 18.61 and 4.4 year modulations in high sea levels at 258 tide gauge sites around the world [see *Menéndez and Woodworth*, 2010, Figure 10], although this was not the focus of their study. The period from 1970 onward was considered. They noted the limitation of estimating nodal amplitudes from only two cycles of data in the records commencing in 1970. They found significant (90% confidence) signals for the nodal component with ranges of up to 0.1 m in the northeast Atlantic and the South China Sea. They found significant signals for the 4.4 year modulation along the coastlines of North America, the South China Sea, and several locations in eastern and southern Australia, with ranges of less than 0.06 m. Comparing *Menéndez and Woodworth*'s [2010] Figure 10 with Figure 4 shows that the geographically limited coverage of the GESLA tide gauge network does not capture the spatial complexity of the tidal modulations and therefore highlights the advantage of the modeling approach employed in this current study. Our results are qualitatively consistent with those of *Menéndez and Woodworth* [2010] at the tide gauge locations. However, a direct comparison of the range of the two modulations is difficult because of differences between the tidal levels examined and data lengths used. We have focused on the annual 99.9th percentile level for a 60 year period, whereas *Menéndez and Woodworth* [2010] estimated the magnitude of the tidal modulations from time series of monthly maxima with varying lengths. As highlighted in section 4.1, the amplitudes of the tidal modulations are sensitive to the tidal level chosen. A more direct, quantitative comparison using the GESLA data and the methods outlined in this paper will form the basis for future work.

[47] The focus of this study has been the contribution of the 18.61 year nodal cycle and 8.85 year perigean cycle to high tidal levels. However, interannual tidal modulations, in particular, nodal modulations, are of special interest in a range of studies and have been linked to changes in sea surface temperature [*Loder and Garrett*, 1978; *Garrett*, 1979], tree ring data (a proxy for air temperatures) [*McKinnell and Crawford*, 2007], monsoonal activity [*Campbell et al.*, 1983], rainfall [*Vines*, 1982], fish populations [*Parker et al.*, 1995], discharge and flooding of the Nile River [*Hameed*, 1984], and coastal and estuarine morphology [*Oost et al.*, 1993; *Jeuken et al.*, 2003; *Gratiot et al.*, 2008]. Hence, the results of this study may have wider implications.

6. Conclusions

[48] This paper has analyzed modeled tides to map the contribution of the 18.61 year lunar nodal cycle and the 8.85 year cycle of lunar perigee (which affects high tidal levels as a quasi 4.4 year cycle) to high tidal levels on a global scale. Regions of the world's oceans where these interannual modulations make the highest contribution to high tidal levels have been identified. The spatial variations in the range and phase of the tidal modulations have been related to the distribution of the main tidal constituents and the form factor and range of the tide. Results have shown that the nodal modulation is largest (between 0.5 and 0.8 m in the 99.9th percentile tidal level) in diurnal regions with tidal ranges of >4 m, and the 4.4 year modulation is largest (between 0.3 and 0.6 m in the 99.9th percentile tidal level) in semidiurnal regions where the tidal range is >6 m. In areas where the form factor of the tide is >~0.6, the nodal modulation dominates over the 4.4 year modulation in high tidal levels, and the phase of the nodal modulation correlates with $N = 0°$ (i.e., maximum lunar declination). In these regions, the nodal modulation was at a maximum in 2006 and will peak again in 2024. In areas where the form factor of the tides is <~0.6, the 4.4 year modulation dominates over the nodal modulation in high tidal levels. In these regions, the phase of the nodal modulation correlates with $N = 180°$ (i.e., minimum lunar declination), and the nodal modulation was maximum in 1997 and will peak again in 2015. The phase of the 4.4 year modulation has also been shown to relate to the form of the tide at a given location. A comparison of the modeled results presented in this paper with the measured quasi-global tide gauge data set GESLA will form the basis for future work.

[49] **Acknowledgments.** We are very grateful to Philip Woodworth and John Hunter for providing comments on an early draft of this paper and for many discussions regarding the results. We would like to thank Lana Erofeeva and Gary Egbert for providing information regarding the TPXO7.2 tidal model and the Tidal Model Driver MATLAB toolbox. We are also grateful to Steve Dickman, an anonymous reviewer, and the editor for their helpful comments and suggestions, which significantly strengthened the paper. This study was funded through the Western Australian Marine Science Institution.

References

Andersen, O. B. (1995), Global ocean tides from ERS 1 and TOPEX/POSEIDON altimetry, *J. Geophys. Res.*, *100*(C12), 25,249–25,259, doi:10.1029/95JC01389.

Araújo, I. B., and D. T. Pugh (2008), Sea levels at Newlyn 1915–2005: Analysis of trends for future flooding risks, *J. Coastal Res.*, *24*(4C), 203–212, doi:10.2112/06-0785.1.

Bradley, J. (1728), An account of a new discovered motion of the fixed stars, *Philos. Trans. R. Soc. London B*, *35*, 637–661, doi:10.1098/rstl.1727.0064.

Campbell, W. H., J. B. Blechman, and R. A. Bryson (1983), Long-period tidal forcing of Indian monsoon rainfall: An hypothesis, *J. Clim. Appl. Meteorol.*, *22*(2), 287–296, doi:10.1175/1520-0450(1983)022<0287:LPTFOI>2.0.CO;2.

Cartwright, D. E. (1974), Years of peak astronomical tides, *Nature*, *248* (5450), 656–657, doi:10.1038/248656a0.

Cartwright, D. E., and A. C. Edden (1973), Corrected tables of tidal harmonics, *Geophys. J. R. Astron. Soc.*, *33*(3), 253–264, doi:10.1111/j.1365-246X.1973.tb03420.x.

Cartwright, D. E., and R. J. Tayler (1971), New computations of the tide-generating potential, *Geophys. J. R. Astron. Soc.*, *23*(1), 45–73, doi:10.1111/j.1365-246X.1971.tb01803.x.

Cherniawsky, J. Y., M. G. G. Foreman, S. Kuh Kang, R. Scharroo, and A. J. Eert (2010), 18.6-year lunar nodal tides from altimeter data, *Cont. Shelf Res.*, *30*(6), 575–587, doi:10.1016/j.csr.2009.10.002.

Doodson, A. T. (1921), The harmonic development of the tide-generating potential, *Proc. R. Soc. London, Ser. A*, *100*(704), 305–329, doi:10.1098/rspa.1921.0088.

Egbert, G. D., and S. Y. Erofeeva (2002), Efficient inverse modeling of barotropic ocean tides, *J. Atmos. Oceanic Technol.*, *19*(2), 183–204, doi:10.1175/1520-0426(2002)019<0183:EIMOBO>2.0.CO;2.

Egbert, G. D., A. F. Bennett, and M. G. G. Foreman (1994), TOPEX/POSEIDON tides estimated using a global inverse model, *J. Geophys. Res.*, *99*(C12), 24,821–24,852, doi:10.1029/94JC01894.

Eliot, M. (2010), Influence of interannual tidal modulation on coastal flooding along the Western Australian coast, *J. Geophys. Res.*, *115*, C11013, doi:10.1029/2010JC006306.

Foreman, M. G. G. (1977), Manual for tidal heights analysis and prediction, *Pac. Mar. Sci. Rep. 77-10*, 58 pp., Inst. of Ocean Sci., Patricia Bay, Sidney, B. C., Canada. [Available at http://www.omg.unb.ca/GGE/5013_LABS/heights.pdf.]

Foreman, M. G. G., and E. T. Neufeld (1991), Harmonic tidal analyses of long time series, *Int. Hydrogr. Rev.*, *LXVIII*(1), 85–108.

Garrett, C. (1979), Mixing in the ocean interior, *Dyn. Atmos. Oceans*, *3*(2–4), 239–265, doi:10.1016/0377-0265(79)90011-3.

Godwin, G. (1972), *The Analysis of Tides*, 264 pp., Univ. of Toronto Press, Toronto, Ont., Canada.

Gratiot, N., E. J. Anthony, A. Gardel, C. Gaucherel, C. Proisy, and J. T. Wells (2008), Significant contribution of the 18.6 year tidal cycle to regional coastal changes, *Nat. Geosci.*, *1*(3), 169–172, doi:10.1038/ngeo127.

Haigh, I., R. Nicholls, and N. Wells (2010), Assessing changes in extreme sea levels: Application to the English Channel, 1900–2006, *Cont. Shelf Res.*, *30*(9), 1042–1055, doi:10.1016/j.csr.2010.02.002.

Hameed, S. (1984), Fourier analysis of Nile flood levels, *Geophys. Res. Lett.*, *11*(9), 843–845, doi:10.1029/GL011i009p00843.

Jeuken, M. C. J. L., Z. B. Wang, D. Keiller, I. Townend, and G. A. Liek (2003), Morphological response of estuaries to nodal tide variation, paper presented at International Conference on Estuaries and Coasts, Int. Network on Erosion and Sedimentation, Hangzhou, China. [Available at http://www.irtces.org/pdf-hekou/018.pdf.]

Kaye, C. A., and G. W. Stuckey (1973), Nodal tidal cycle of 18.6 yr.: Its importance in sea-level curves of the East Coast of the United States and its value in explaining long-term sea-level changes, *Geology*, *1*(3), 141–144, doi:10.1130/0091-7613(1973)1<141:NTCOYI>2.0.CO;2.

Loder, J. W., and C. Garrett (1978), The 18.6-year cycle of sea surface temperature in shallow seas due to variations in tidal mixing, *J. Geophys. Res.*, *83*(C4), 1967–1970, doi:10.1029/JC083iC04p01967.

Lowe, J. A., et al. (2010), Past and future changes in extreme sea levels and waves, in *Understanding Sea-Level Rise and Variability*, edited by J. A. Church et al., pp. 326–375, Wiley-Blackwell, London.

Marmer, H. A. (1951), *Tidal Datum Planes*, *Spec. Publ. 135*, 142 pp., U.S. Gov. Print. Off., Washington, D. C.

McKinnell, S. M., and W. R. Crawford (2007), The 18.6-year lunar nodal cycle and surface temperature variability in the northeast Pacific, *J. Geophys. Res.*, *112*, C02002, doi:10.1029/2006JC003671.

Menéndez, M., and P. L. Woodworth (2010), Changes in extreme high water levels based on a quasi-global tide-gauge data set, *J. Geophys. Res.*, *115*, C10011, doi:10.1029/2009JC005997.

Nicholls, R. J., P. P. Wong, V. R. Burkett, J. O. Codignotto, J. E. Hay, R. F. McLean, S. Ragoonaden, and C. D. Woodroffe (2007), Coastal systems and low-lying areas, in *Climate Change 2007: Impacts, Adaptation and Vulnerability, Contribution of Working Group II to the Fourth Assessment Report of the Intergovernmental Panel on Climate Change*, edited by M. L. Parry et al., pp. 315–356, Cambridge Univ. Press, Cambridge, U. K.

Oost, A. P., H. de Haas, F. Ijnsen, J. M. van den Boogert, and P. L. de Boer (1993), The 18.6 yr nodal cycle and its impact on tidal sedimentation, *Sediment. Geol.*, *87*(1–2), 1–11, doi:10.1016/0037-0738(93)90032-Z.

Parker, K. S., T. C. Royer, and R. B. Deriso (1995), High-latitude climate forcing and tidal mixing by the 18.6-year lunar nodal cycle and low-frequency recruitment trends in Pacific halibut (*Hippoglossus stenolepis*), in *Climate Change and Northern Fish Populations*, edited by R. J. Beamish, *Can. Spec. Publ. Fish. Aquat. Sci.*, *121*, 447–459.

Pugh, D. J. (1987), *Tides, Surges and Mean Sea-Level: A Handbook for Engineers and Scientists*, 472 pp., John Wiley, Chichester, U. K.

Pugh, D. T. (2004), *Changing Sea Levels: Effects of Tides, Weather and Climate*, 280 pp., Cambridge Univ. Press, Cambridge, U. K.

Ray, R. D. (2007), Decadal climate variability: Is there a tidal connection?, *J. Clim.*, *20*(14), 3542–3560, doi:10.1175/JCLI4193.1.

Shaw, A. G. P., and M. N. Tsimplis (2010), The 18.6 yr nodal modulation in the tides of southern European coasts, *Cont. Shelf Res.*, *30*(2), 138–151, doi:10.1016/j.csr.2009.10.006.

Shum, C. K., et al. (1997), Accuracy assessment of recent ocean tide models, *J. Geophys. Res.*, *102*(C11), 25,173–25,194, doi:10.1029/97JC00445.

Simon, B. (2007), *La Marée Océanique Côtière*, 433 pp., Inst. Océanogr., Paris.

Vines, R. G. (1982), Rainfall patterns in the western United States, *J. Geophys. Res.*, *87*(C9), 7303–7311, doi:10.1029/JC087iC09p07303.

Wood, F. (2001a), *Tidal Dynamics*, vol. 2, *Extreme Tidal Peaks and Coastal Flooding*, 389 pp., Coastal Educ. Res. Found., West Palm Beach, Fla.

Wood, F. (2001b), *Tidal Dynamics*, vol. 1, *Theory and Analysis of Tidal Forces*, 326 pp., Coastal Educ. Res. Found., West Palm Beach, Fla.

Woodworth, P. L., and D. L. Blackman (2004), Evidence for systematic changes in extreme high waters since the mid-1970s, *J. Clim.*, *17*(6), 1190–1197, doi:10.1175/1520-0442(2004)017<1190:EFSCIE>2.0.CO;2.

Woodworth, P. L., D. L. Blackman, D. T. Pugh, and J. M. Vassie (2005), On the role of diurnal tides in contributing to asymmetries in tidal probability distribution functions in areas of predominantly semi-diurnal tide, *Estuarine Coastal Shelf Sci.*, *64*(2–3), 235–240, doi:10.1016/j.ecss.2005.02.014.

M. Eliot, I. D. Haigh, and C. Pattiaratchi, School of Environmental Systems Engineering and UWA Oceans Institute, University of Western Australia, M470, 35 Stirling Hwy., Crawley, WA 6009, Australia. (haigh@sese.uwa.edu.au)